

Reconnection remnants in the magnetic cloud of October 18–19, 1995: A shock, monochromatic wave, heat flux dropout, and energetic ion beam

Michael R. Collier,¹ A. Szabo,¹ W. M. Farrell,¹ J. A. Slavin,¹ R. P. Lepping,¹
R. Fitzenreiter,¹ B. Thompson,¹ D. C. Hamilton,² G. Gloeckler,²
G. C. Ho,³ P. Bochsler,⁴ D. Larson,⁵ and L. Ofman⁶

Abstract. Evidence is presented that the Wind spacecraft observed particle and field signatures on October 18–19, 1995, due to reconnection near the foot points of a magnetic cloud (i.e., between 1 and 5 solar radii). These signatures include (1) an internal shock traveling approximately along the axis of the magnetic cloud, (2) a simple compression of the magnetic field consistent with the foot point magnetic fields being thrust outward at speeds much greater than the solar wind speed, (3) an electron heat flux dropout occurring within minutes of the shock, indicating a topological change resulting from disconnection from the solar surface, (4) a very cold 5 keV proton beam, and (5) an associated monochromatic wave. We expect that given observations of enough magnetic clouds, Wind and other spacecraft will see signatures similar to the ones reported here indicating reconnection. However, these observations require the spacecraft to be fortuitously positioned to observe the passing shock and other signatures and will therefore be associated with only a small fraction of magnetic clouds. Consistent with this, a few magnetic clouds observed by Wind have been found to possess internal shock waves.

1. Introduction

Magnetic clouds are a subset of interplanetary ejecta characterized by strong magnetic fields which exhibit a smooth, large rotation taking of the order of 1 day at 1 AU and low proton temperatures. They are currently of great interest in part because of their association with coronal mass ejections (CMEs) and because of their magnetospheric impact [Burlaga *et al.*, 1981; Laakso *et al.*, 1998; Moore *et al.*, 1999]. Magnetic clouds typically expand at about half the Alfvén speed and, because of their adiabatically decreasing magnetic field, are expected to disappear somewhere between 2 and 12 AU [Osherovich *et al.*, 1993], although this has not clearly been demonstrated in the literature. With the fleet of satellites at 1 AU resulting from the International Solar Terrestrial Physics (ISTP) program, magnetic cloud observations from solar origin through geomagnetic effect are now possible [e.g., Fox *et al.*, 1998].

The large-scale geometry of magnetic clouds is well described by a force-free magnetic field represented by a set of helical field lines called a flux rope [Burlaga, 1995; Wu *et al.*,

1995; Low and Hundhausen, 1995; Osherovich *et al.*, 1999]. However, there appear to be smaller-scale physical processes occurring within magnetic clouds [Christon *et al.*, 1998; Takeuchi *et al.*, 1998].

Because magnetic cloud foot points are hypothesized to be frequently still attached to the Sun, we might expect to observe signatures on magnetic cloud field lines of time-dependent processes in the lower corona. One such time-dependent process is magnetic reconnection, which effects the disconnection of the foot points [Gosling *et al.*, 1995]. Indeed, Gosling [1990] posits this as the basic process by which interplanetary flux ropes are formed: Namely, the helical flux rope topology of these CMEs is created after the CME liftoff from the corona as a natural consequence of three-dimensional magnetic reconnection of rising magnetic loops. On the other hand, there are also authors [Marubashi, 1997; Bothmer and Rust, 1997] who point out that the flux ropes could be convected outward rather than being formed by the reconnection process during the liftoff of CMEs from the Sun. However, reconnection is likely to occur in the aftermath of both scenarios.

This paper is organized as follows: Section 2 provides an overview of the October 1995 magnetic cloud. Section 3 gives a cursory overview of reconnection theory. Section 4 addresses the Magnetic Field Investigation (MFI) magnetic field data describing the shock, the upstream and downstream wave activity, and the propagation direction of the shock. Section 5 details the results of a variance analysis applied to the monochromatic wave data. Here we discuss the monochromatic wave polarization and propagation direction. Section 6 introduces Wind Three-Dimensional Plasma (3DP) data and shows a clear Doppler shift associated with this monochromatic wave. The Doppler shift allows a determination of the wave plasma frame frequency and the magnitude of the \mathbf{k} (wave) vector. Section 7 describes Wind High Mass Resolution Spectrometer

¹Space Sciences Directorate, NASA Goddard Space Flight Center, Greenbelt, Maryland.

²University of Maryland, College Park.

³Applied Physics Laboratory, The Johns Hopkins University, Laurel, Maryland.

⁴University of Bern, Bern, Switzerland.

⁵University of California, Berkeley.

⁶Laboratory for Astronomy and Solar Physics, Raytheon Information Technology and Scientific Services and NASA Goddard Space Flight Center, Greenbelt, Maryland.

Copyright 2001 by the American Geophysical Union.

Paper number 2000JA000101.
0148-0227/01/2000JA000101\$09.00

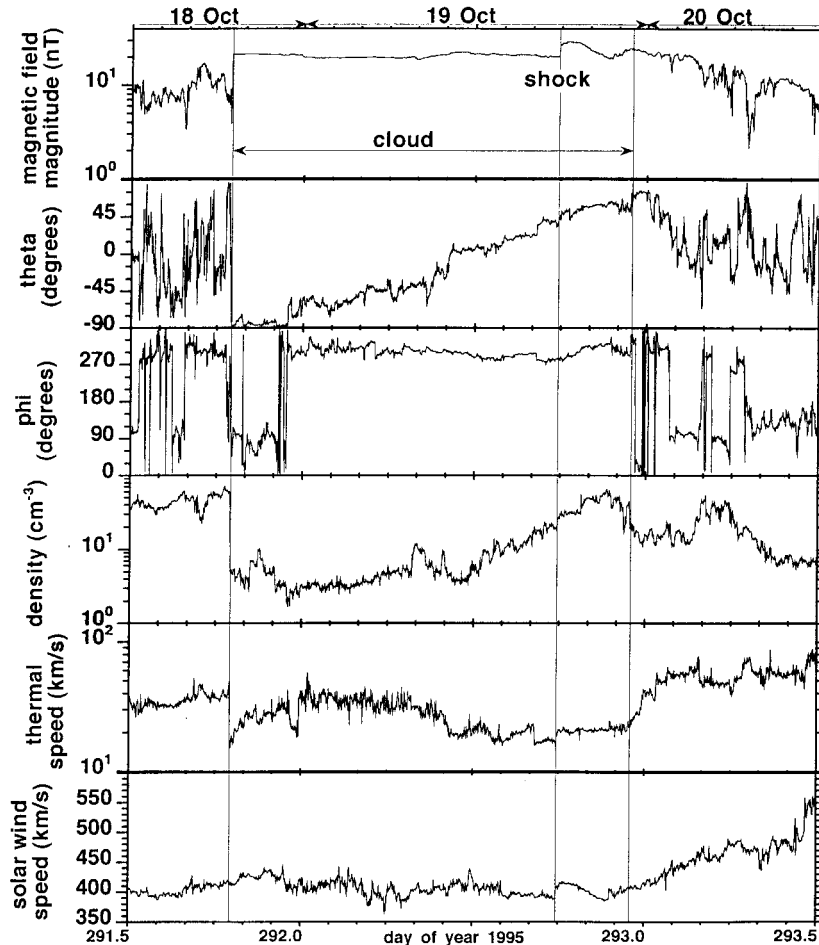


Figure 1. Overview of the Wind MFI and SWE magnetic field and plasma observations during the October 18–19, 1995, magnetic cloud. The interior of the cloud is marked with the two-headed arrow, although there is some ambiguity about the location of the back of the cloud. The internal shock is most evident in the magnetic field magnitude, in the first panel, whereas the magnetic field direction, given in the second and third panels, varies little across the shock. The density, thermal speed, and velocity all increase across this shock, so that it shows characteristics of a fast forward MHD shock. The shock speed is very close to the Alfvén speed, approximately the fast-mode speed.

(MASS) data which show that associated with this shock was a cold 5 keV proton beam. Section 8 discusses anisotropy information obtained from the MASS instrument. Section 9 shows that the Wind Solar Wind Experiment (SWE) instrument observed an electron heat flux dropout associated with the shock, indicating a topology change. Section 10 addresses some issues dealing with shock orientation and propagation. Section 11 interprets the observations as resulting from the foot point of the magnetic cloud reconnecting close to the Sun. Section 12 uses the Wind MASS observations along with a simple coronal model to place the reconnection site between 1 and 5 solar radii. Finally, section 13 provides a brief conclusion.

2. October 1995 Cloud

One example of a well-studied magnetic cloud was observed by the Wind spacecraft on October 18–19, 1995. An overview of the magnetic field and plasma parameters during this time is shown in Figure 1. The first three panels display Wind magnetic field data from the Magnetic Field Investigation (MFI) [Lepping *et al.*, 1995], with the upper panel showing the mag-

netic field magnitude in nanoteslas on a logarithmic scale (see Figure 1 of Lepping *et al.* [1995] for a linear scale). The next two panels show in degrees the magnetic field angle out of the ecliptic plane, θ , and in the ecliptic plane, ϕ (with 0° pointing toward the Sun). The interior of the cloud is indicated by the two-headed arrow between the vertical lines. Although there is some ambiguity about the location of the back of the cloud, it does not bear on this analysis, so we have only indicated one of the possible boundaries [Lepping *et al.*, 1997]. This cloud is of type southward-westward-northward (SWN), that is, right-handed helicity, and according to Bothmer and Rust [1997] should have had its origin in the southern hemisphere of the Sun [Bothmer and Schwenn, 1998; Z. Smith *et al.*, 1997].

This cloud has been fit using a force-free “constant α ” helical flux rope model resulting in cylindrical Bessel functions:

$$B_\phi = B_0 J_1(\alpha r), \quad (1)$$

$$B_z = B_0 J_0(\alpha r), \quad (2)$$

where B_ϕ and B_z are the azimuthal and axial fields, respectively, B_0 is the central field, r is the distance from the cloud

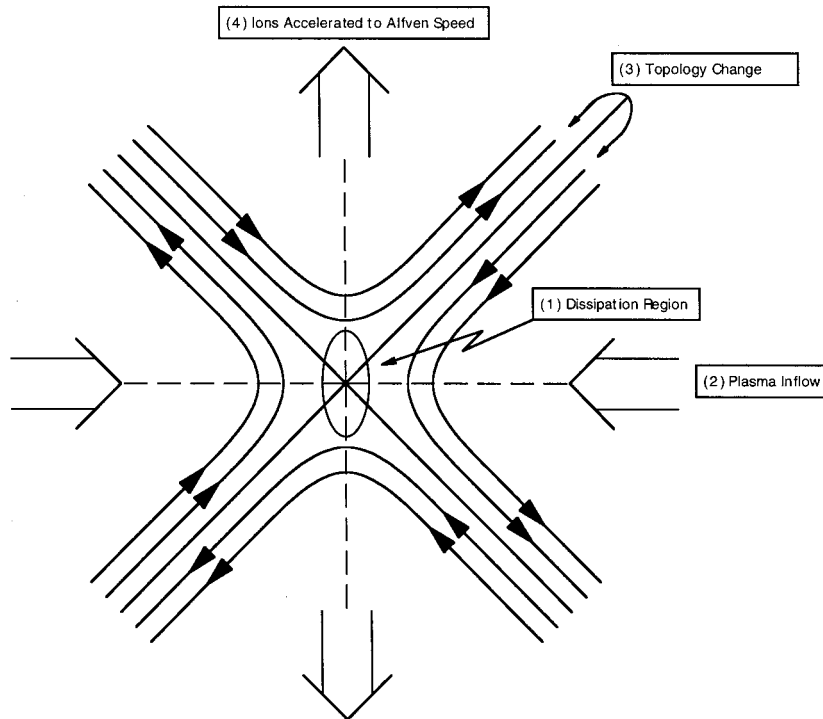


Figure 2. Reconnection process at an X-type neutral line. (1) Magnetic field and plasma are accelerated in the diffusion region. (2) The magnetic field lines and plasma enter from the left and right and are ejected toward the top and bottom. (3) This causes a topology change. (4) The ions are preferentially accelerated to the Alfvén speed.

axis, and α is a constant relating the current and magnetic field ($\alpha \mathbf{B} = \nabla \times \mathbf{B}$) [Burlaga, 1995; Priest, 1987].

The fitting result was awarded a rating of “1: excellent” on the subjective Lepping quality scale. This scale includes the ranks 1 for “excellent,” 2 for “good,” 3 for “poor,” and “cl” for “cloud-like,” indicating that the helical flux rope fitting is unlikely to be successful for any reasonable model. Of 34 magnetic clouds identified by R. P. Lepping using Wind data from 1995–1998 (including the October 1995 cloud), 13 were rated “excellent” (rank 1), 15 were rated “good” (rank 2), 5 were rated “poor” (rank 3), and 1 was rated “cloud-like” (rank cl), so that in terms of fit quality, this cloud is in about the upper one third [Lepping *et al.*, 1990, 1997] (see also magnetic cloud data available from Wind MFI team, NASA Goddard Space Flight Center, at http://lepmfi.gsfc.nasa.gov/mfi/mag_cloud_pub1.html#table).

Note that the magnetic field strength during the cloud interval is considerably higher than typical interplanetary values at 1 AU. Although there is no dramatic change in ϕ , the angle θ rotates steadily from pointing below to pointing above the ecliptic. The internal shock occurs slightly before 1800 UT and manifests itself as a significant jump in the magnetic field magnitude although the angles θ and ϕ remain largely unaffected.

The Solar Wind Experiment (SWE) density, thermal speed, and solar wind speed are shown in the bottom three panels of Figure 1 [Ogilvie *et al.*, 1995]. At the time of the internal shock the density, thermal speed, and solar wind speed all abruptly increase, so that this internal shock has the characteristics of a typical fast forward MHD interplanetary shock. Lepping *et al.* [1997] refer to this as a “shock-in-formation,” a compression still steepening into a shock, or a shock-like structure which seems to compress the magnetic field. We will simply refer to

it as a shock. The magnetic field direction, as illustrated in Figure 1, shows little change as the shock ramp passes Wind. Hence it appears to be a perpendicular shock. The field is undergoing simple compression. Although it could be argued that the cause of this internal shock was the high-speed stream following the cloud, this interaction would likely produce a shock orientation close to the radial direction. However, as will be discussed in more detail in sections 4 and 10, the orientation of this shock is far from the radial direction.

In addition, inside this magnetic cloud and just downstream of the interplanetary shock an unusually monochromatic wave of ~ 1 s period was observed. Data from the Wind MASS instrument show that at the time of this wave there was a very cold 5 keV proton beam present, and energetic electron pitch angle data from the Wind SWE instrument show that all these unusual observations were associated with a topology change. This time period within the October 18–19, 1995, magnetic cloud is the subject of this paper.

3. Reconnection Theory

Magnetic reconnection, a process believed to operate in and around planetary magnetospheres as well as in the solar corona, releases stored magnetic energy in the form of high-velocity streams of ions and electrons and also heats up the particles. Figure 2 shows a simplified diagram of reconnection at an X-type neutral line [Kivelson and Russell, 1995]. (1) This process is believed to result from resistivity breaking the frozen-in constraint within a small “dissipation region” which forms around the X line as shown in Figure 2. (2) Magnetic field lines and plasma enter the diffusion region from the side and leave from the top and bottom. (3) This effects a topology

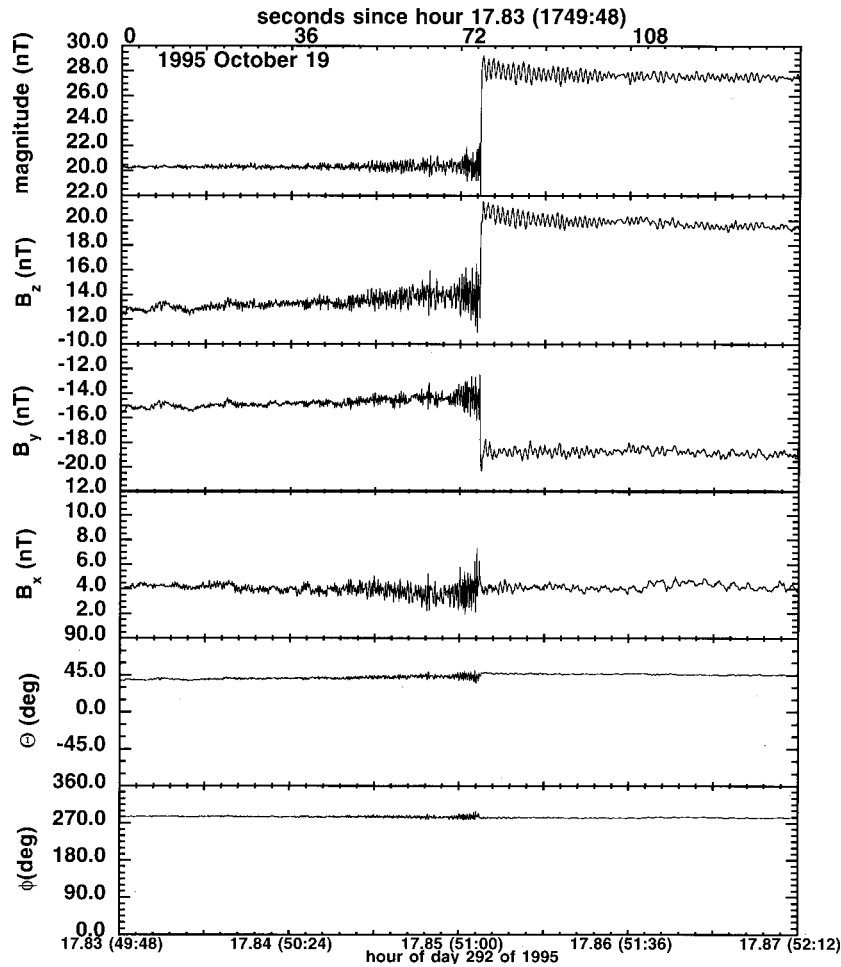


Figure 3. Overview of the MFI high-resolution (11 vectors every second) magnetic field data showing the “shock” inside the October 18–19 magnetic cloud. The top panel shows the magnetic field magnitude in nanoteslas with the second through fourth panels showing the individual GSE components of the magnetic field. The fifth and sixth panels show the θ (out of the ecliptic) and ϕ (in the ecliptic) angles of the magnetic field. The shock transition occurs between 1751:425 and 1751:436 UT on day 292 (October 19) with the monochromatic wave immediately following and lasting ~ 30 s. There is pronounced high-frequency wave activity ($\gg 1$ Hz) present on the upstream side. Note that the magnetic field angle changes very little during this time period.

change in which the field lines connect to different partners. (4) Within the diffusion region the ions are accelerated away from the X line, reaching the Alfvén speed in the outflow region [Shay *et al.*, 1999].

In the Petschek [1964] solution the acceleration occurs as the plasma passes through slow-mode shock waves connected to the diffusion region. This innovation increased the magnetic reconnection rate to realistic levels. A further refinement was made by Sonnerup [1970], who introduced fast-mode shocks to loosen the inflow speed constraint on the Petschek model [Kivelson and Russell, 1995].

Thus, for the purpose of this work, reconnection carries with it a number of signatures: (1) shocks associated with the reconnection process; (2) topological changes which are frequently deduced by changing particle populations associated with different flux tubes [Gosling *et al.*, 1990] (here, topological changes are indicated by the presence or absence of field-aligned and anti-field-aligned halo electrons); and (3) ions preferentially accelerated to the Alfvén speed [Kessel *et al.*, 1996].

It is, however, unclear how far away from the reconnection region the signatures can still be detected, and, indeed, not all signatures will survive from the Sun to 1 AU if reconnection near the Sun is the source of the observed features. This may explain why not all shocks internal to magnetic clouds show the signatures reported here. We do argue, though, that the presence of the magnetic cloud serves to duct the shocks and makes them observable at large distances from the Sun.

4. MFI Magnetic Field Data

Figure 3 shows MFI magnetic field data late in hour 17 of day 292 (October 19), 1995, around the time of the internal shock. The duration of the plot is ~ 2 min. The data are high resolution; MFI supplies ~ 11 magnetic field vectors every second at this time. The shock feature, between 1751:425 UT and 1751:436 UT, makes its transition in less than a tenth of a second. Prior to the transition, in the upstream region, there is pronounced high-frequency wave activity, while after the transition there are low-frequency, nearly monochromatic waves

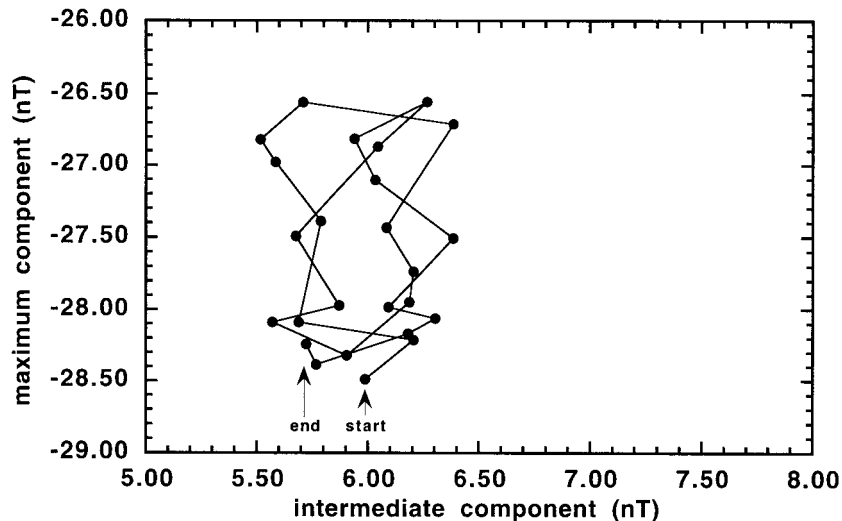


Figure 4. Hodogram showing maximum versus intermediate component for the “first” 25 data points of the wave. The eigenvalue ratios of the variance analysis are $\lambda_{\text{int}}/\lambda_{\text{min}} = 2.0$ and $\lambda_{\text{max}}/\lambda_{\text{int}} = 5.7$, so that the propagation direction is not exceptionally well determined. Note that the wave appears to be elliptically polarized.

which, at first sight, may appear to be an instrumental or analysis-related artifact. This type of signature can creep into the data, sometimes as a result of incompletely accounting for spin modulation. We have examined these possibilities and are confident that the wave is real.

During the time period immediately following the shock transition the amplitude of the wave starts out at close to 1 nT but decays quickly over the course of ~ 30 s. Some residual activity is apparent for at least another 30 s after this plot, although at significantly reduced levels. This is common for the Earth’s fast-mode bow shock because of waves being generated by thermalizing ions in the shock ramp.

Using data from Geotail, which observed parts of this magnetic cloud when the bow shock oscillated past the spacecraft, *Lepping et al.* [1997] found a propagation direction for this internal shock which is within $\sim 20^\circ$ of the cloud axis. The cloud axis is oriented at $(0.351, -0.913, -0.203)$ in GSE coordinates, and the shock normal is oriented at $(-0.558, 0.714, 0.423)$. Consequently, it appears that this shock is actually traveling along the magnetic cloud, rather than through it, suggestive of a “ducting” mode with the origin at the foot points of the cloud.

5. Variance Analysis

Figure 4 is a hodogram showing the maximum versus intermediate component of the magnetic field obtained from a variance analysis [*Sonnerup and Cahill*, 1967] performed on the “first” 25 data points (~ 2.5 s) of the wave. Five data points

immediately after the wave rose were eliminated because they “wandered,” perhaps because the wave had not completely developed by the time of these five data points. Figure 4 shows the wave to be elliptically polarized, as one might in general expect.

The minimum variance direction obtained from the variance analysis which we interpret as the propagation direction is

$$\hat{\mathbf{n}} = (0.565, -0.599, -0.567), \quad (3)$$

where the three components are the GSE x , y , and z directions, respectively, and the field direction is

$$\hat{\mathbf{b}} = (0.147, -0.671, 0.726), \quad (4)$$

so that $\hat{\mathbf{b}} \cdot \hat{\mathbf{n}} = 0.073$ ($\theta = 85.8^\circ$), so that the wave appears to be propagating almost perpendicularly to the magnetic field (consistent with the bottom two panels of Figure 3, which show little direction change in the magnetic field) but parallel to the shock normal (within 11°) and parallel to the magnetic cloud axis (within 30°). The eigenvalue ratios were $\lambda_{\text{max}}/\lambda_{\text{min}} = 11.7$ and $\lambda_{\text{int}}/\lambda_{\text{min}} = 2.0$, so that the propagation direction is not well determined. For example, *Lepping and Behannon* [1980] claim that when $\lambda_{\text{int}}/\lambda_{\text{min}} < 1.8$, the normal is too poorly determined to be useful, and we are close to that. However, the inferred propagation direction fits into our interpretation reasonably well as this propagation direction is consistent with the shock being the source of this monochromatic wave.

Table 1 summarizes the relevant structure angles based on analysis from both this work and *Lepping et al.* [1997] (see their Figure 10 for an overview of the angles). To a reasonable approximation, the shock normal, magnetic cloud axis, and wave propagation directions are aligned and perpendicular to the magnetic field direction.

Thus this is a possible electrostatic wave propagating almost perpendicularly to the ambient field. Such waves may be important for filling the quasi-linear gap at 90° ; that is, they will efficiently scatter particles with large pitch angles [*Karimabadi et al.*, 1992].

Table 1. Matrix of Angles

	Cloud Axis	Shock Normal	Wave Propagation	Magnetic Field
Shock normal	159° (\parallel)
Wave propagation	31° (\parallel)	169° (\parallel)
Magnetic field	59° (\perp)	105° (\perp)	86° (\perp)	...
Radial (GSE x)	69° (\perp)	124° (\perp)	56° (\perp)	82° (\perp)

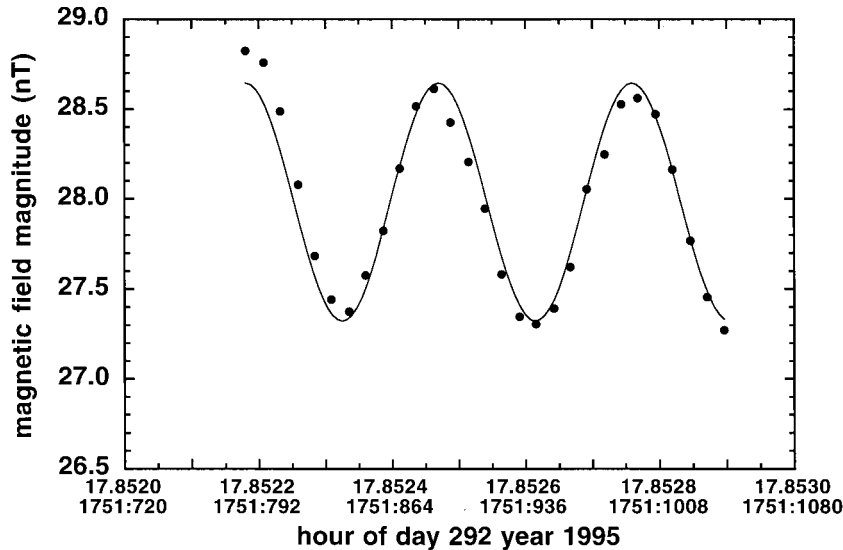


Figure 5. An example of a sine fit to a 3 s interval of MFI high-resolution magnetic field magnitude data. The shock jump occurs at 1751:436 UT with the wave significantly damped by \sim 1751:3348 UT. The wave duration was 23.1 s, and the functional form fit was $m_1 + m_2 \cos [3600 m_3 (m_0 - t_{\text{start}})]$, where t_{start} is the beginning of the 3 s data interval. Phase was eliminated by starting and ending on a complete half cycle. The values for m_1 , m_2 , and m_3 , as well as the start time used for each of the eight fits, are listed in Table 2.

6. 3DP Plasma Data

In this study, we use high-resolution plasma data from the 3DP instrument [Lin *et al.*, 1995]. Specifically, the most appropriate data set is proton velocity, which is obtained at \sim 3 s resolution. These solar wind speeds have been compared to the SWE and Solar Wind and Suprathermal Ion Composition Investigation (Solar Wind Ion Composition Spectrometer (SWICS)/MASS/Suprathermal Ion Composition Spectrometer (STICS)) (SMS) MASS data, and although the time resolution of the SWE and MASS instruments is significantly lower than that of 3DP, the level of agreement is reasonably good, to \sim 5%. This level of agreement in the absolute value of the solar wind speed provides great confidence in the relative changes in solar wind speed observed by 3DP and used in this study.

Because of the monochromatic nature of this wave, Fourier decomposition was unnecessary. Instead, to determine wave period, a simple sine wave was conveniently fit to the magnetic field magnitude and described the data well. Fits were done during the first 23.1 s of magnetic field data following the shock transition when the wave was most evident, prior to being damped out.

Because the intention was to compare the magnetic field wave data to plasma data from the 3DP instrument, which yields a measurement every 3 s, 3 s magnetic field data intervals were selected for fitting to a sine function. Figure 5 shows a typical fit to a 3 s segment of MFI high-resolution data. Table 2 lists the fit parameters corresponding to the eight fits performed to the magnetic field data. Here m_1 is a constant offset, m_2 is the amplitude, and m_3 is the frequency.

Figure 6 shows a plot of the observed wave frequency versus solar wind speed, which, of course, is primarily in the GSE x direction. The data are reasonably described by a linear relationship with a positive slope (although with great uncertainty in the parameters), indicating Doppler shifting of the observed frequency with solar wind speed. A fit to the straight line

$$\omega_{\text{obs}} = k v_{\text{sw}} \cos \theta_{k v_{\text{sw}}} - \omega_0, \quad (5)$$

using a value for $\cos \theta_{k v_{\text{sw}}}$ of 0.565 from (3), where v_{sw} is the solar wind speed, allows a determination of the wavelength $\lambda = 2\pi/k$ and the frequency in the solar wind rest frame $\nu_0 = \omega_0/2\pi$. The fit shown in Figure 6 indicates that $k = 0.19 \pm 0.07 \text{ km}^{-1}$. This implies a wavelength $\lambda = 33 \text{ km}$ which is relatively close to the shock ramp thickness determined by Lepping *et al.* [1997] of 62 km. The plasma frame frequency $\omega_0 = 39.7 \pm 17.7 \text{ rad s}^{-1}$ ($\nu_0 = 6.3 \text{ s}^{-1}$). As is apparent from an inspection of Figure 6, there is significant uncertainty in both of these values. These values imply a phase velocity of $\omega_0/k = 209 \pm 121 \text{ km s}^{-1}$.

7. MASS Particle Beam Observations

The high-resolution electrostatic mass spectrometer MASS, part of the SMS (SWICS/MASS/STICS) package on the Wind spacecraft, was designed so that the particles pass through a spherical deflection system prior to entering the time-of-flight assembly [Gloeckler, 1990; Gloeckler *et al.*, 1995; Hamilton *et al.*, 1990]. Consequently, by using start signal counts, the MASS instrument can function as a standard energy per charge analyzer and can determine solar wind speeds, proton and alpha particle densities and temperatures, and suprathermal particle characteristics [Collier *et al.*, 1996, 1998]. Over each spacecraft spin period (\sim 3 s) the voltage on the deflection

Table 2. Fit Parameters

Fit	m_1 , nT	m_2 , nT	m_3 , rad s $^{-1}$	Start Time, UT
a	27.99	0.66	6.03	1751:785
b	27.80	0.75	6.10	1751:1109
c	27.73	-0.63	5.98	1751:1382
d	27.71	-0.49	6.37	1751:1696
e	27.68	-0.62	6.46	1751:2009
f	27.65	0.49	6.24	1751:2329
g	27.62	0.46	6.41	1751:2635
h	27.65	0.25	6.61	1751:2938

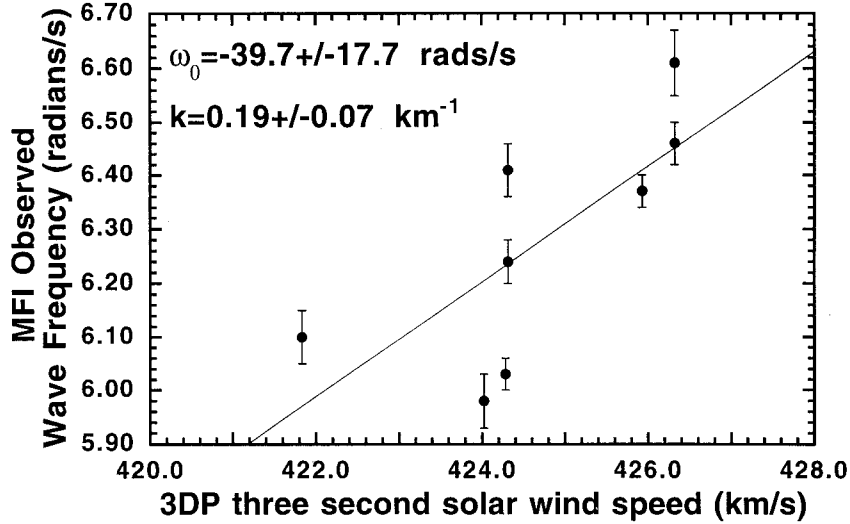


Figure 6. The observed frequencies in the Wind spacecraft frame obtained from the magnetic field sine fits (an example of which is shown in Figure 5) plotted versus the observed 3DP 3 s solar wind speed data. If the Doppler shift is assumed to obey $\omega_{\text{obs}} = k v_{\text{sw}} \cos \theta_{k v_{\text{sw}}} + \omega_0$, where k is the wave vector and ω_0 is the rest frame wave frequency, then the fit given by the solid line provides $\omega_0 = -39.7 \pm 17.7 \text{ rad s}^{-1}$ and $k = 0.19 \pm 0.07 \text{ km}^{-1}$. The correlation coefficient for these data is 0.73.

plates changes to scan 60 values, so that an entire scan takes ~ 3 min and covers logarithmically an energy per charge range of $0.52\text{--}9.89 \text{ keV } e^{-1}$ with a 4% passband.

During the approximately 30 s when the wave intensity was greatest (1751:06–1751:33 UT) the MASS instrument scanned the energy per charge range from ~ 3.5 to $5.4 \text{ keV } e^{-1}$. Figure

7 shows the background-adjusted front secondary electron detection assembly rate 2 (FSR2) count rate, which is unsectored, that is, contains no directional information.

A statistically significant peak occurs at an energy per charge of $\sim 5 \text{ keV } e^{-1}$. If it is assumed that this peak represents a minor ion convecting at the same speed as helium (minor ions

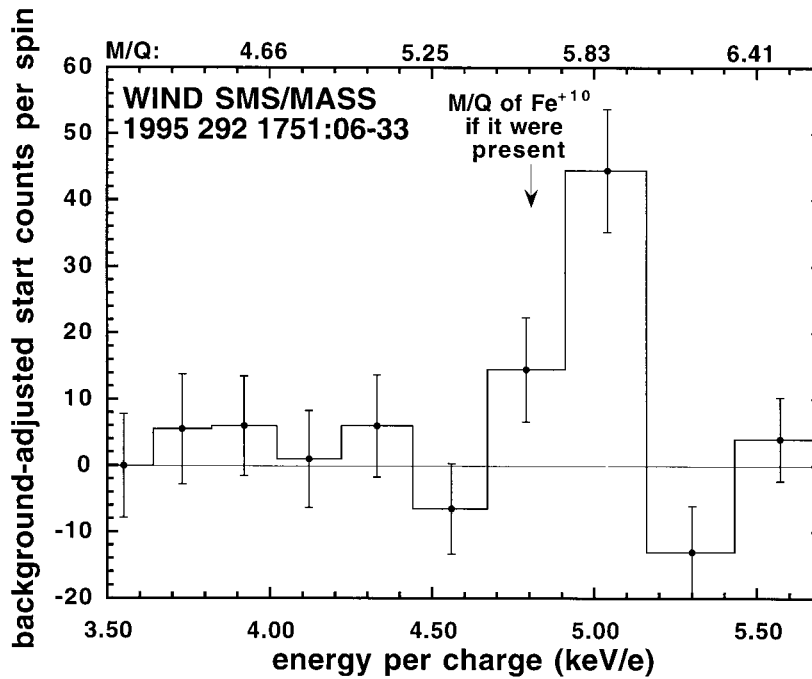


Figure 7. The background-adjusted SMS MASS FSR2 count rate during the wave time period (1751:06–1751:33 UT). The time periods used for background subtraction were 1745:00–1745:28 and 1754:09–1754:37 UT, which cover the same energy per charge range. A clear, statistically significant peak occurs at an energy per charge of $\sim 5 \text{ keV } e^{-1}$. The mass per charge (M/Q, indicated at the top of the plot) corresponding to iron of charge state +10 is indicated by the arrow, although it is argued that the beam is probably suprathermal protons.

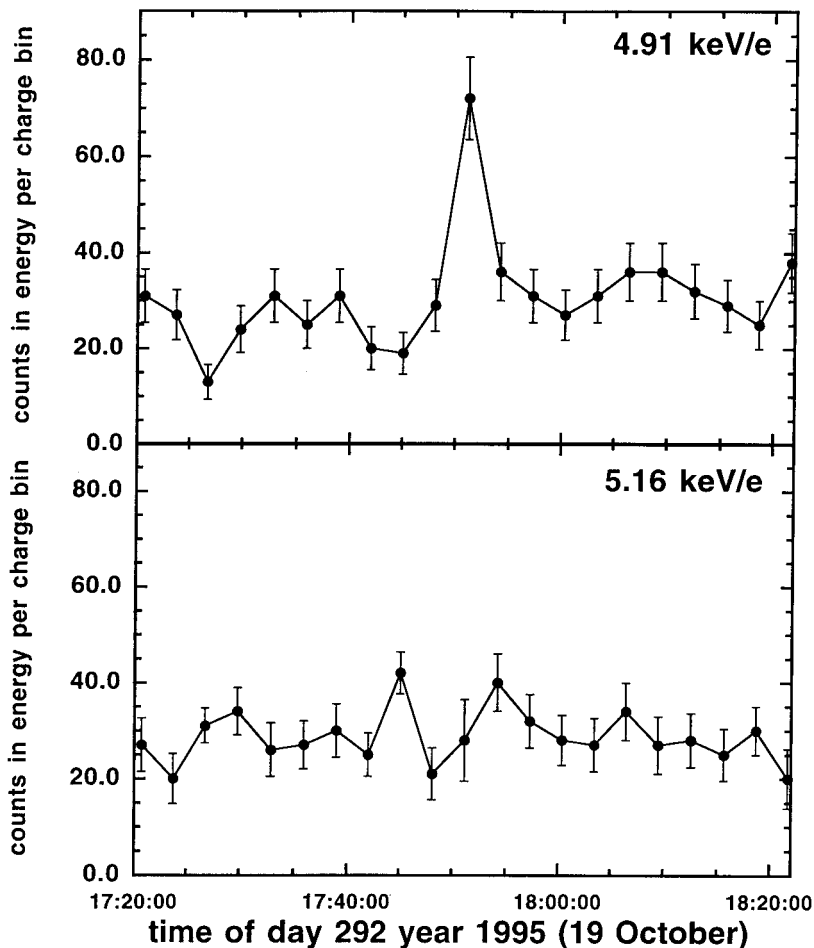


Figure 8. Counts in the $4.91 \text{ keV } e^{-1}$ and $5.16 \text{ keV } e^{-1}$ energy per charge bins as a function of time over a 1 hour interval from 1720–1820 UT. The beam is very “narrow” in velocity space.

tend to convect at the helium speed rather than the proton speed), then the species mass per charge would be ~ 5.83 . This could correspond roughly to iron with charge state +10 (mass per charge $(M/Q) = 56/10 = 5.6$), not an atypical charge state for iron in the solar wind [Gloeckler *et al.*, 1999]. Although elements, and, in particular, iron, with unusual charge state distributions have been observed in magnetic clouds [Gloeckler, 1998; Burlaga *et al.*, 1998; Skoug *et al.*, 1999], it is highly unlikely that iron of only this charge state would be enhanced and not the adjacent charge states, +9 and +11 [Henke *et al.*, 1998]. Figure 7 shows their conspicuous absence ($M/Q = 56/9 = 6.22$ and $56/11 = 5.09$, as shown on the upper x axis).

Consequently, we propose that this enhancement is most likely a 5 keV proton beam accelerated by a reconnection process close to the Sun. It is well known that a two-species, three-component plasma composed of thermal ions and electrons and an ion beam is unstable and will lead to wave growth [Gary *et al.*, 1984]. It is also well known that upstream of shocks, “back streaming” and “diffuse” ion populations are observed [Ipavich *et al.*, 1984; Möbius *et al.*, 1986].

The two-paneled Figure 8 shows, as a function of time, the unsectored FSR2 count rate for the $4.91 \text{ keV } e^{-1}$ bin (top panel) and the $5.16 \text{ keV } e^{-1}$ bin (bottom panel). The highest count rate that the $4.91 \text{ keV } e^{-1}$ channel attained over the entire 28 hour magnetic cloud was during the 30 s monochromatic wave period. Note that (1) the statistical significance of

the beam enhancement in the top panel is at the 3σ – 4σ level and (2) the beam is very “narrow.” It has a low temperature and a high Mach number; that is, the relative width in energy is less than the instrument passband width ($\Delta E/E \leq 0.051$). This determines the lower limit on the velocity over the velocity spread, or the thermal Mach number ($v/\Delta v \geq 2/0.051 = 39.3$).

Finally, these ion observations contain only the energy range scanned by the MASS instrument over the 30 or so seconds during which the wave occurred (spanning 3.46 – $5.43 \text{ keV } e^{-1}$). This is a small fraction of the total energy range MASS scans every 3 or so minutes (0.52 – $9.89 \text{ keV } e^{-1}$). Consequently, the possibility of other ion beams or interesting features outside the observed 3.46 – $5.43 \text{ keV } e^{-1}$ band cannot be ruled out.

Lutsenko and Kudela [1999] have reported more than 200 cases of “almost monoenergetic ions” of very short duration, of the order of 1 min, with energies between 30 and 600 keV associated with spacecraft connection to the bow shock. Although we do not believe that the monoenergetic beam we observe has a similar physical origin (because the beam we observe is narrower and lower in energy, the wave is only on one side of the shock, and there was no change in the magnetic field direction across the shock), their observations are important because they hint that contrary to the predictions of the standard shock-associated particle models [Ipavich *et al.*, 1981;

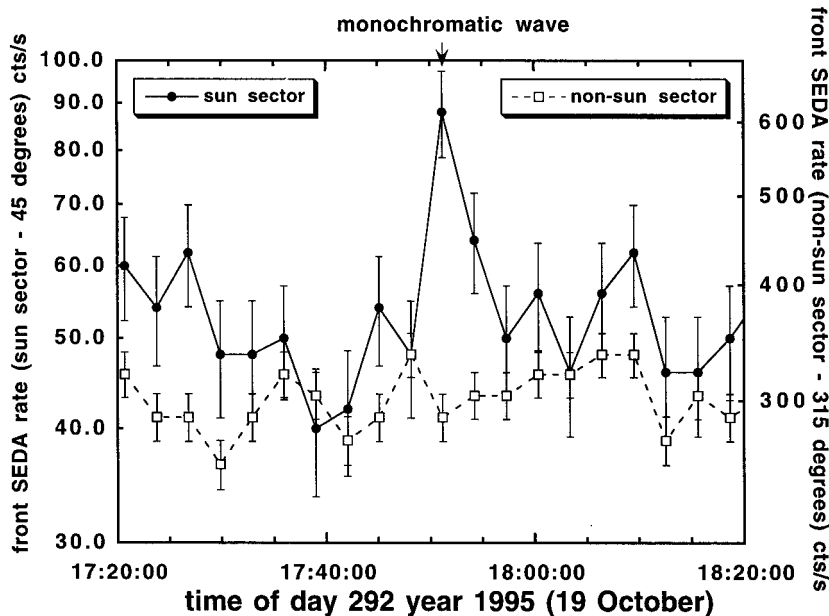


Figure 9. The sectored front secondary electron detection assembly (SEDA) rate for both the 45° Sun and the 135° non-Sun sectors for the energy per charge bin $4.91 \text{ keV } e^{-1}$ are plotted on the left and right y axes, respectively. The logarithmic y axes are offset by a factor of 7 to account for the disparate angular ranges of the two sectors.

Lee, 1982], shocks may produce high-energy nearly monochromatic beams.

One possible interpretation of the data involves an $\sim 5 \text{ kV}$ shock potential. The higher-frequency (upstream) nonmonochromatic waves could then be created by reflected ions off the potential. These reflected ions would, in turn, create a counter, unstable stream in the solar wind. Also, the energy of this counterstream would be lower ($< 5 \text{ keV}$), thereby resonating with the higher-frequency waves and explaining why the emission appears at higher frequency. As far as the downstream monochromatic wave goes, the low temperature of the 5 keV beam may explain the monochromatic nature of the wave. However, the shock potential is generally some fraction of the upstream ion ram kinetic energy [Mandt and Kan, 1991], so that 5 kV may be excessively large. Thus reconnection appears to be the most reasonable explanation for this monoenergetic beam.

8. Monoenergetic Beam Anisotropies

Figure 9 shows, during an hour interval which includes the monochromatic wave period, the sectored front secondary electron detection assembly rate for the 45° Sun sector, which observes flow approximately along the negative GSE x direction, and for the 315° non-Sun sector, which is sensitive to particles coming from all other directions. Not surprisingly, there is a slight background anisotropy ($a_1 \approx 0.089 \pm 0.062$) in approximately the solar wind direction, which may be simply a Compton-Getting effect due to the solar wind flow [Ipavich, 1974]. However, at the time of the monochromatic wave there is a dramatic increase in the particle anisotropy ($a_1 = 0.363$), indicating a strong anisotropy in the 45° Sun sector, centered on the Sun-Earth line.

Particles streaming parallel to the shock normal, which is oriented at $\sim 128^\circ$ with respect to the GSE x axis, would all be

observed at $\sim 52^\circ$ off the Sun-Earth line and hence in the 315° MASS non-Sun sector. Because these particles are observed primarily in the Sun sector and the magnetic field is primarily in the GSE y - z plane, we conclude that these particles have relatively large pitch angles. However, these anisotropy results are based on only two sectors, whose averages could alias fine structure in the angular distributions.

These observations may explain why the cold proton beam and the shock arrive at the same time even though they are not traveling at the same speed (the shock speed in the solar wind frame is 137 km s^{-1} , and the proton beam is traveling at $\sim 1000 \text{ km s}^{-1}$). Although it could be argued that their coincidence suggests a local origin for the beam, the shock propagates perpendicularly to the magnetic field lines whereas the particles must navigate the highly helical structure of the magnetic cloud to arrive at the spacecraft and hence have traveled significantly farther. In addition, the anisotropy measurements indicate that these particles carry a large pitch angle, so that the component of their velocity along the magnetic field is somewhat less than 1000 km s^{-1} , further contributing to a longer travel time for the particles than if they were freely moving perpendicularly to the field lines as the shock does.

9. SWE Electron Heat Flux Measurements

The presence of energetic electrons greater than $\sim 100 \text{ eV}$ or so streaming parallel and/or antiparallel to the magnetic field is generally viewed as a signature of foot points connected to the Sun, the putative source of the electron heat flux [Gosling, 1990; Larson et al., 1997]. During the course of the magnetic cloud, Wind experienced a variety of different topologies from closed on both ends, to closed on one end, to open on both ends [Janoo et al., 1998; Crooker et al., 1998] with each open field line presumably associated with a reconnection event

similar to the events discussed by *Gosling et al.* [1995] and *Bothmer et al.* [1996].

Larson et al. [1997] interpret the 3DP electron data during this cloud passage as evidence for patchy disconnection of one or both ends of the cloud magnetic field lines from the Sun. The analysis of *Larson et al.* [1997] is not alone in suggesting reconnection inside the cloud. *Janoo et al.*'s [1998] results may also be interpreted in this manner.

Plate 1 shows Wind SWE electron pitch angle distributions during a 20 min period including the time of the monochromatic wave at four energies, 94, 139, 203, and 298 eV. Prior to the time of the shock the electrons appear to be streaming antiparallel to the magnetic field, indicating connection to the Sun on one end of the magnetic cloud. The shock appears to broaden the pitch angle distribution somewhat, and ~ 9 min later the 180° pitch angle electrons disappear, indicating that the topology of the magnetic cloud has transitioned from being connected on one end to being disconnected on both ends, presumably because of a reconnection event. In fact, this may be the strongest argument for reconnection associated with this internal shock. As further evidence supporting this interpretation, the internal shock is moving away from the recently reconnected side of the cloud, as expected if reconnection is the source of the disturbance.

In general, observed changes in magnetic cloud topology evidenced by the electron pitch angle distributions are interpreted as being due to the spacecraft moving between flux tubes with different topologies and are not associated with magnetic field, plasma, and energetic particle signatures similar to the ones seen around 1750 UT in the October 19, 1995, cloud. In order to observe these reconnection signatures the spacecraft must be on the correct field line at whatever time the shock passes. Before the time near shock passage the field lines will appear to be connected, and following the time near shock passage, the field lines will appear to be disconnected. There is a short "window of opportunity," but if this interpretation is correct, eventually other magnetic clouds should be found which show similar shock or shock-like structures.

In fact, a cursory examination of magnetic field data from 34 magnetic clouds observed by Wind between 1995 and 1998 has found three cases, including the October 1995 case discussed here, of shocks internal to magnetic clouds. So, it appears, although the statistics are rather poor, that internal shocks may manifest themselves in $\sim 10\%$ or so of magnetic clouds observed at 1 AU.

In addition, the magnetometer on Ulysses appears to have observed a shock internal to a magnetic cloud at ~ 5 AU late on day 228 in 1997 [*Forsyth et al.*, 1999], so that this phenomenon is not restricted to 1 AU.

10. Shock Orientation

One of the unusual features of this internal shock is its orientation, which is roughly perpendicular to the magnetic field and antiparallel to the cloud axis (see Table 1). *Chao et al.* [1999] have suggested that the origin of this internal shock is an X-ray flare located at 9°N , 54°W on October 16, 1995, at 1221 UT and claim that the interaction of this solar interplanetary disturbance with the magnetic cloud would produce the observed shock orientation. In this section, we examine solar data not to prove the scenario we propose but in an attempt to see if the alternative scenario of *Chao et al.* is supported.

The literature has established that fast CMEs, and not flares,

are the source of interplanetary shocks. However, CMEs are often accompanied by flares, so, indeed, a CME may have been associated with the flare on October 16, 1995. A rough estimate assuming constant propagation shows that the cloud should have started on the Sun in the afternoon hours of October 14, 1995. Indeed, a filament disappearance on this day located at 11°S , 14°E from 1543 to 1634 UT is believed to be the source of this cloud [*Chao et al.*, 1999]. We might expect the shock then to have had its origin about a day later. However, shocks often decelerate, so that it is at least plausible that it may have been caused by a CME on October 16, 1995.

This is, however, difficult to conclude unambiguously, and for a number of reasons we believe reconnection near the foot points of the CME to be a more natural explanation for the observations as a whole as well as for the shock orientation: (1) The electron observations indicate a topology change which is not predicted by the mechanism proposed by *Chao et al.* [1999]. (2) The direction of the shock motion is consistent with an origin at the side of the cloud attached to the Sun initially, as deduced from the electron observations (although the direction of shock motion is also consistent with the *Chao et al.* scenario). (3) The energetic ion observations are consistent with reconnection close to the solar surface, which is not predicted by the mechanism proposed by *Chao et al.* (4) The GOES data values for the flare which *Chao et al.* propose as effecting the internal shock are extremely small, barely above background, and may not actually qualify by post-Solar and Heliospheric Observatory (SOHO) standards as a "flare." Also, it could be argued that flares are not the best way to look for CMEs that would drive a shock and that frequently very small flares can have CMEs with them.

As a further check, Yohkoh soft X-ray telescope (SXT) data were examined (N. Nitta, private communication, 1999). The standard signatures of a CME viewed by SXT include expanding active region loops, filament eruptions, and other signs of material or ejecta leaving the Sun [*Hudson and Webb*, 1997; *Hudson et al.*, 1998]. One of the more reliable signatures is a coronal "dimming," a lack of emission above or in the proximity of the erupting region, which is interpreted as indicating the removal of material from the corona and frequently serves ipso facto as evidence of a CME [*Hudson et al.*, 1996]. The filament eruptions appear primarily through a related effect, arcade formation. The arcades form during or after an eruption, and in the event that the neutral line is extended, the arcades are typically collinear about the neutral line. Additionally, any change in coronal magnetic field topology (e.g., "sigmoid" disappearances and arcade formation) which might have an extended reach may be indicative of CMEs. The exception to this rule is flaring regions which are not associated with CMEs; that is, CMEs may have flares, but flares alone cannot be used as indicators of CMEs (the exception being the "two-ribbon flare," which corresponds to the extended neutral line collinear arcades). In any case, there is no evidence in the Yohkoh SXT data suggesting a CME.

Finally, we consulted the Mauna Loa data (J. Burkepile, private communication, 1999) for any reports of CMEs. Their white light observations on October 16, 1995, began at ~ 1726 UT, 5 hours following the flare at 1221 UT, and it is quite possible that 5 hours after the flare a CME would be visible in the Mauna Loa field of view, although the data are not very conclusive because of the observational gaps. Furthermore, Mauna Loa is better at detecting limb CMEs than Earth-directed CMEs. Nevertheless, their observing logs report "no

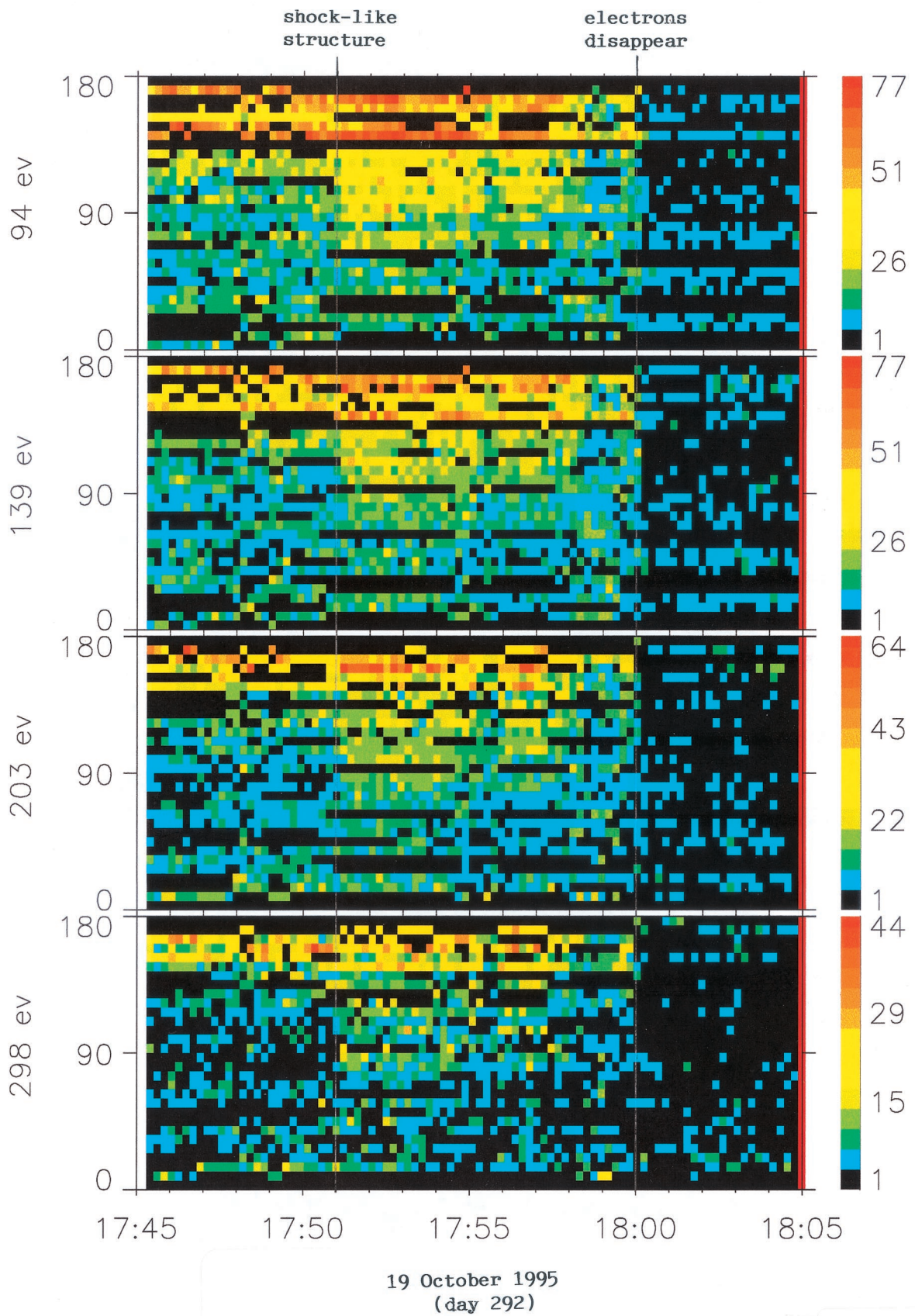


Plate 1. Wind SWE electron pitch angle distributions around the time of the internal shock-like feature. The four panels show four energies: 94, 139, 203, and 298 eV. Prior to the shock the electrons appear to be primarily streaming at 180° pitch angle. The shock appears to broaden the pitch angle distribution, and ~9 min after the shock the streaming electrons disappear.

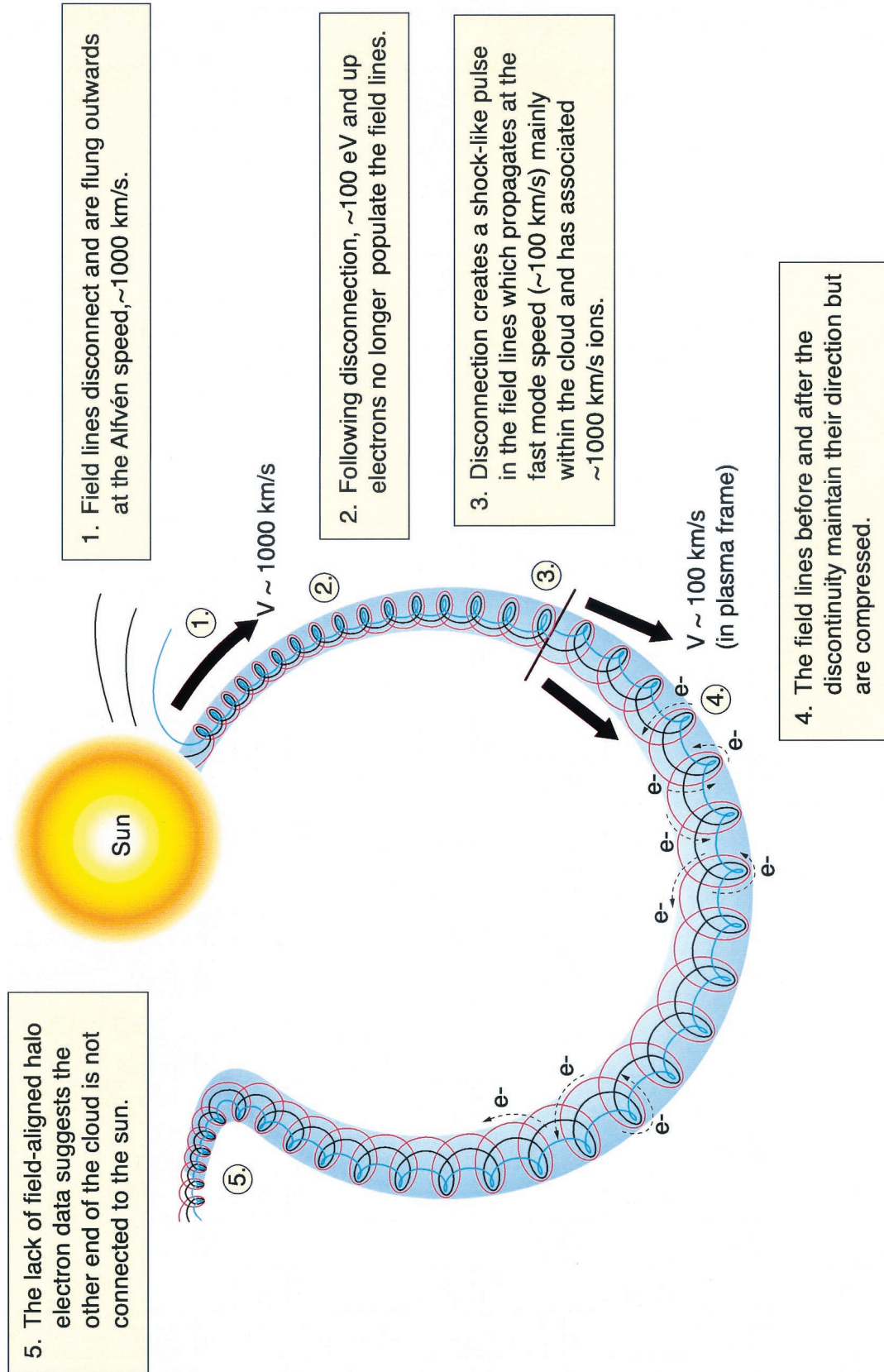


Plate 2. Schematic summary of the reconnection interpretation for the Wind observations inside the magnetic cloud of October 18–19, 1995. Initially, a field line disconnects from the solar surface and is flung outward at ~ 1000 km s⁻¹, the Alfvén speed, accelerating ions which are later observed by the Wind spacecraft to this speed (corresponding to ~ 5 keV). The reconnection event triggers a disturbance in the field lines which propagates along the cloud axis at the fast-mode speed. The field lines before and after the discontinuity maintain their direction, but are compressed. Because the presence of halo electrons indicates connection to the solar surface, following the disconnection, ~ 100 eV and up electrons no longer populate the field lines.

coronal activity” for that day. In summary, although a small flare occurred on October 16, 1995, we have been unable to find any conclusive evidence for a CME, let alone a CME driving a shock, which is necessary for the *Chao et al.* [1999] mechanism.

Finally, because the main motivation of the proposal of *Chao et al.* [1999] was to explain this internal shock’s unusual shock normal direction (56° with the negative GSE x axis) by postulating an additional interacting shock off the side of the cloud, it should be pointed out that because we expect magnetic clouds to “duct” fast-mode waves, the shock orientation is also consistent with the reconnection interpretation, as stated in section 4.

Wave ducting is a well-accepted process for coronal loops close to the Sun [*Ireland*, 1996; *J. M. Smith et al.*, 1997]. The fast-mode speed is significantly higher inside the cloud than outside because of its higher magnetic field strength and lower density, so the phase fronts will move more quickly within the cloud. Furthermore, the flux rope geometry provides that propagation near the boundary is frequently quasi-perpendicular to the magnetic field and hence travels faster than the parallel direction [*Hu*, 1998]. Finally, dissipative processes such as viscous dissipation which prevent disturbances from propagating far from their source may be most effective in weak field regions [*Roberts et al.*, 1984; *Gordon and Hollweg*, 1983]. It may be the case that only disturbances in strong field regions (such as in a magnetic cloud) propagate far from their point of origin [*McLean et al.*, 1971].

11. Reconnection Model

The reconnection interpretation of these observations is summarized by Plate 2, which illustrates a few field lines (red, black, and blue) in the magnetic cloud. According to the electron pitch angle data, Plate 1, which shows anti-field-aligned energetic electron fluxes coming only from one direction, initially one leg of the field is attached to the solar surface while the other has already reconnected. Then, the following steps occur: (1) Field lines close to the solar surface reconnect and are flung outward at the local Alfvén speed, $\sim 1000 \text{ km s}^{-1}$ (the speed of the proton beam observed by MASS), along with the particles on the field lines at the time. This explains the MASS observations of $\sim 5 \text{ keV}$ protons associated with the shock: They reflect the Alfvén speed at the reconnection site. This beam may also supply the free energy for the monochromatic wave. Note that we interpret the monochromatic wave as resulting from the weak shock and ion beam, so that the presence of the wave is not essential to the reconnection argument. The reconnected field lines initially move much more rapidly than the solar wind, accelerating the solar wind downstream of the disturbance and creating the slight increase in solar wind speed associated with the increase in magnetic field strength. (2) Following the reconnection process, the halo electrons can no longer populate the field lines. (3) The reconnection creates a disturbance in the field lines which propagates mainly within the cloud (because of the reasons cited in section 10) at the local fast-mode speed (the shock velocity in the solar wind frame is 137 km s^{-1} , and the Alfvén speed is 120 km s^{-1}). Thus the shock observed within the cloud is propagating approximately along the cloud axis (see Table 1). (4) Because the reconnected field lines are thrust outward at $\sim 1000 \text{ km s}^{-1}$ and the field lines in front of them are traveling more slowly, the field after the shock passes maintains the same direction

but is compressed and increases in magnitude as observed in the data shown in Figure 3. (5) The lack of field-aligned halo electrons suggests that throughout this process the other end of the magnetic field lines in the part of the magnetic cloud being observed at this time was not attached to the Sun.

12. Coronal Model and Reconnection Location

If this reconnection interpretation is correct, then the observed proton beam speed of $\sim 1000 \text{ km s}^{-1}$ represents approximately the Alfvén speed at the point of reconnection. To determine the range of distances from the solar surface that such an Alfvén speed may mark, we examine a simple isothermal hydrostatic two-fluid coronal model described by

$$T \frac{\partial \rho}{\partial r} = - \frac{GM_\odot m_p}{r^2} \rho + eE \quad (6)$$

for the protons and

$$T \frac{\partial \rho}{\partial r} = -eE \quad (7)$$

for the electrons. Here, T is the temperature, ρ is the density, G is the universal gravitational constant, M_\odot is the solar mass, m_p is the proton mass, and r is the distance from the Sun. Although taking the electron and proton temperatures to be identical constitutes a bad assumption in the solar wind, for the purpose of determining the Alfvén speed it is not critical because the mass density is determined by the protons and the scale height is determined by the average of the proton and electron temperatures.

Subtracting the two equations allows a determination of the electric field

$$E = \frac{GM_\odot m_p}{2r^2 e} \rho. \quad (8)$$

Plugging this back into the ion equation (6) and solving for the density yields

$$\rho(r) = \rho_0 \exp \left\{ - \frac{1.15 \times 10^7}{T|_K} \left(1 - \frac{r_0}{r} \right) \right\}, \quad (9)$$

where $T|_K$ is the temperature in Kelvin. If the expansion is assumed to be radial and flux is conserved, then the magnetic field magnitude may be determined by

$$B(r) = B_0 \left(\frac{r_0}{r} \right)^2, \quad (10)$$

and the Alfvén speed v_A may be determined by using the relation

$$v_A = \frac{B}{\sqrt{\mu_0 \rho}} = 892 \frac{B}{\sqrt{\rho}}, \quad (11)$$

where B is in teslas, ρ is in kg m^{-3} , and v_A is in m s^{-1} .

Using this model with a reasonable range of values for T , ρ_0 , and B_0 at 1 solar radius produces an Alfvén speed of $\sim 1000 \text{ km s}^{-1}$ (the speed of the proton beam observed by MASS) at a distance of between 1 and 5 or so solar radii. Figure 10 shows the model results for Alfvén speed and density for $T = 1.6 \times 10^6 \text{ K}$, $\rho_0 = 1.7 \times 10^{-12} \text{ kg m}^{-3}$, and $B_0 = 1.3 \times 10^{-3} \text{ T}$. The $1.3 \times 10^{-3} \text{ T}$ magnetic field value represents a radial extrapolation of the observed 28 nT Wind field

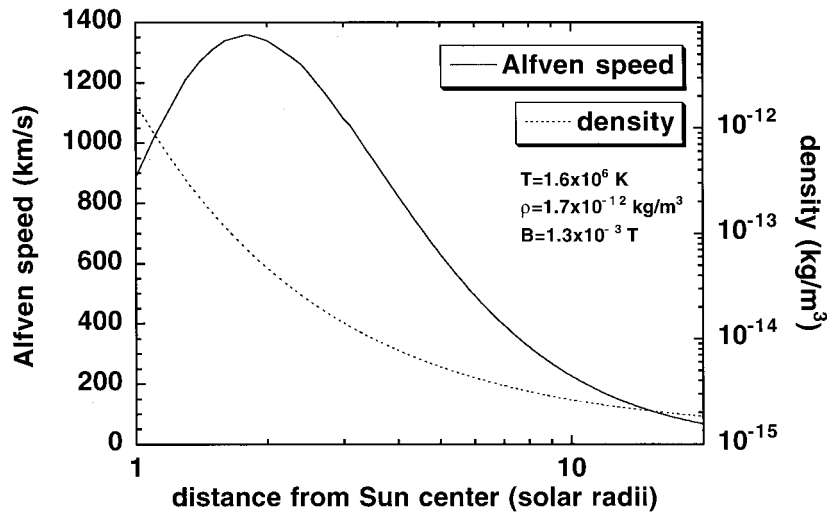


Figure 10. Sample results for the Alfvén speed and the density as a function of distance from the solar surface for a simple isothermal hydrostatic two-fluid coronal model using a coronal temperature of 1.6×10^6 K, a density of 1.7×10^{-12} kg m $^{-3}$, and a magnetic field of 1.3×10^{-3} T. This model is used to place the location of the reconnection point between 1 and 5 solar radii. The 1 solar radius field value used represents a radial extrapolation of the 28 nT field observed at Wind back to the Sun and as such represents a lower bound for the field at the Sun since most probably the field expands superradially.

back to the solar surface. As the field probably expands super-radially, this likely underestimates the field somewhat. Also, because the slow (i.e., equatorial) solar wind flow is believed to be subsonic to ~ 4 solar radii, the inclusion of solar wind flow will not affect the model Alfvén speed significantly in the region of interest. These radial distances for reconnection are reasonable and support the scenario that Wind is observing reconnection remnants inside the October 18–19, 1995, magnetic cloud.

13. Conclusion

We have presented Wind observations from MFI, 3DP, SMS, and SWE inside the October 18–19, 1995, magnetic cloud which may be interpreted as evidence of reconnection occurring at low altitudes in the solar corona, between 1 and 5 solar radii. The observations include an internal shock traveling approximately along the axis of the magnetic cloud, simple compression of the magnetic field consistent with the foot point magnetic fields being thrust outward at speeds much greater than the solar wind speed, an electron heat flux drop-out occurring within minutes of the shock, indicating a topological change resulting from disconnection from the solar surface, and a very cold 5 keV proton beam resulting from reconnection. In addition, an unusually monochromatic wave propagating perpendicularly to the magnetic field was observed in association with the shock and may be related to the monoenergetic particle beam. It is clear that reconnection must take place to avoid a continuous buildup of magnetic flux in the heliosphere, but direct evidence of this process is hard to find. This study's uniqueness results from bringing together so many different signatures supporting reconnection in a single event.

Because the spacecraft must be fortuitously positioned to observe the shock when it passes, observations such as the ones reported here will be rare. Furthermore, because shocks will expand, it may be possible to observe a shock internal to a

magnetic cloud without a corresponding topology change or energetic particle beam. Thus a more detailed study is necessary to draw unambiguous conclusions. However, if our interpretation is correct, given observations of enough magnetic clouds with sophisticated instrumentation, similar observations inside magnetic clouds should surface in the future, particularly as we transition to solar maximum and magnetic clouds become more frequent. Consistent with this, a few magnetic clouds have been found to possess internal shocks.

Acknowledgments. This research was performed in part while Michael R. Collier was a National Research Council Resident Research Associate in the Electrodynamic Branch, Code 696, at the NASA Goddard Space Flight Center. Thanks are due to Larry Bleau at the University of Maryland for helping us access MASS data. Thanks are also due to Joan Burkepile and Nariaki Nitta for helping us get data and images. This work was funded in part by the ISTP SOLARMAX Extended Science Program.

Janet G. Luhmann thanks Robert J. Forsyth and Volker Bothmer for their assistance in evaluating this paper.

References

- Bothmer, V., and D. M. Rust, The field configuration of magnetic clouds and the solar cycle, in *Coronal Mass Ejections*, *Geophys. Monogr. Ser.*, vol. 99, edited by N. Crooker, J. Joselyn, and J. Feynman, pp. 139–146, AGU, Washington, D. C., 1997.
- Bothmer, V., and R. Schwenn, The structure and origin of magnetic clouds in the solar wind, *Ann. Geophys.*, 16, 1–24, 1998.
- Bothmer, V., M. I. Desai, R. G. Marsden, T. R. Sanderson, K. J. Trattner, K.-P. Wenzel, J. T. Gosling, A. Balogh, R. J. Forsyth, and B. E. Goldstein, Ulysses observations of open and closed magnetic field lines within a coronal mass ejection, *Astron. Astrophys.*, 316, 493–498, 1996.
- Burlaga, L. F., *Interplanetary Magnetohydrodynamics*, pp. 89–114, Oxford Univ. Press, New York, 1995.
- Burlaga, L., E. Sittler, F. Mariani, and R. Schwenn, Magnetic loop behind an interplanetary shock: Voyager, Helios, and IMP 8 observations, *J. Geophys. Res.*, 86, 6673–6684, 1981.
- Burlaga, L., et al., A magnetic cloud containing prominence material: January 1997, *J. Geophys. Res.*, 103, 277–285, 1998.

- Chao, J. K., C. B. Wang, D. J. Wu, and R. P. Lepping, Interaction of the Oct. 14–19, 1995 magnetic cloud with a solar interplanetary disturbance, *Eos Trans. AGU*, 80(17), Spring Meet. Suppl. S269, 1999.
- Christon, S. P., et al., Concurrent observations of solar wind oxygen by Geotail in the magnetosphere and Wind in interplanetary space, *Geophys. Res. Lett.*, 25, 2987–2990, 1998.
- Collier, M. R., D. C. Hamilton, G. Gloeckler, P. Bochsler, and R. B. Sheldon, Neon-20, oxygen-16, and helium-4 densities, temperatures, and superthermal tails in the solar wind determined with Wind/MASS, *Geophys. Res. Lett.*, 23, 1191–1194, 1996.
- Collier, M. R., D. C. Hamilton, G. Gloeckler, G. Ho, P. Bochsler, R. Bodmer, and R. Sheldon, Oxygen 16 to oxygen 18 abundance ratio in the solar wind observed by Wind/MASS, *J. Geophys. Res.*, 103, 7–13, 1998.
- Crooker, N. U., et al., Sector boundary transformation by an open magnetic cloud, *J. Geophys. Res.*, 103, 26,859–26,868, 1998.
- Forsyth, R. J., A. Balogh, E. J. Smith, and J. T. Gosling, Magnetic field structure of transients at Ulysses: Their relationship to coronal structure and CMEs, paper presented at IUGG99, Int. Union of Geod. and Geophys., Birmingham, England, U. K., 1999.
- Fox, N. J., M. Peredo, and B. J. Thompson, Cradle to grave tracking of the January 6–11, 1997 Sun-Earth connection event, *Geophys. Res. Lett.*, 25, 2461–2464, 1998.
- Gary, S. P., C. W. Smith, M. A. Lee, M. L. Goldstein, and D. W. Fooslund, Electromagnetic ion beam instabilities, *Phys. Fluids*, 27, 1852–1862, 1984.
- Gloeckler, G., Ion composition measurement techniques for space plasmas, *Rev. Sci. Instrum.*, 61, 3613–3620, 1990.
- Gloeckler, G., Solar wind composition measurements from the SWICS and SWIMS instruments on ACE, *Eos Trans. AGU*, 79(17), Spring Meet. Suppl. S259, 1998.
- Gloeckler, G., et al., The solar wind and suprathermal ion composition investigation on the Wind spacecraft, *Space Sci. Rev.*, 71, 79–124, 1995.
- Gloeckler, G., L. A. Fisk, S. Hefti, N. A. Schwadron, T. H. Zurbuchen, F. M. Ipavich, J. Geiss, P. Bochsler, and R. F. Wimmer-Schweingruber, Unusual composition of the solar wind in the 2–3 May 1998 CME observed with SWICS on ACE, *Geophys. Res. Lett.*, 26, 157–160, 1999.
- Gordon, B. E., and J. V. Hollweg, Collisional damping of surface waves in the solar corona, *Astrophys. J.*, 266, 373–382, 1983.
- Gosling, J. T., Coronal mass ejections and magnetic flux ropes in interplanetary space, in *Physics of Magnetic Flux Ropes*, *Geophys. Monogr. Ser.*, vol. 58, edited by C. T. Russell, E. R. Priest, and L. C. Lee, pp. 343–364, AGU, Washington, D. C., 1990.
- Gosling, J. T., M. F. Thomsen, S. J. Bame, T. G. Onsager, and C. T. Russell, The electron edge of the low latitude boundary layer during accelerated flow events, *Geophys. Res. Lett.*, 17, 1833–1836, 1990.
- Gosling, J. T., J. Birn, and M. Hesse, Three-dimensional magnetic reconnection and the magnetic topology of coronal mass ejection events, *Geophys. Res. Lett.*, 22, 869–872, 1995.
- Hamilton, D. C., G. Gloeckler, F. M. Ipavich, R. A. Lundgren, R. B. Sheldon, and D. Hovestadt, New high-resolution electrostatic ion mass analyzer using time of flight, *Rev. Sci. Instrum.*, 61, 3104–3106, 1990.
- Henke, T., J. Woch, U. Mall, S. Livi, B. Wilken, R. Schwenn, G. Gloeckler, R. von Steiger, R. J. Forsyth, and A. Balogh, Differences in the O^{7+}/O^{6+} ratio of magnetic cloud and non-cloud coronal mass ejections, *Geophys. Res. Lett.*, 25, 3465–3468, 1998.
- Hu, Y. Q., Asymmetric propagation of flare-generated shocks in the heliospheric equatorial plane, *J. Geophys. Res.*, 103, 14,631–14,641, 1998.
- Hudson, H. S., and D. F. Webb, Soft X-ray signatures of coronal ejections, in *Coronal Mass Ejections*, *Geophys. Monogr. Ser.*, vol. 99, edited by N. Crooker, J. Joselyn, and J. Feynman, pp. 27–38, AGU, Washington, D. C., 1997.
- Hudson, H. S., L. W. Acton, and S. L. Freeland, A long-duration solar flare with mass ejection and global consequences, *Astrophys. J.*, 470, 629–635, 1996.
- Hudson, H. S., J. R. Lemen, O. C. St. Cyr, A. C. Sterling, and D. F. Webb, X-ray coronal changes during halo CMEs, *Geophys. Res. Lett.*, 25, 2481–2484, 1998.
- Ipavich, F. M., The Compton-Getting effect for low energy particles, *Geophys. Res. Lett.*, 1, 149–152, 1974.
- Ipavich, F. M., A. B. Galvin, G. Gloeckler, M. Scholer, and D. Hovestadt, A statistical survey of ions observed upstream of the Earth's bow shock: Energy spectra, composition, and spatial variation, *J. Geophys. Res.*, 86, 4337–4342, 1981.
- Ipavich, F. M., J. T. Gosling, and M. Scholer, Correlation between the He/H ratios in upstream particle events in the solar wind, *J. Geophys. Res.*, 89, 1501–1507, 1984.
- Ireland, J., Wave heating of the solar corona and SOHO, *Ann. Geophys.*, 14, 485–491, 1996.
- Janoo, L., et al., Field and flow perturbations in the October 18–19, 1995, magnetic cloud, *J. Geophys. Res.*, 103, 17,249–17,259, 1998.
- Karimabadi, H., D. Krauss-Varban, and T. Terasawa, Physics of pitch angle scattering and velocity diffusion, 1, Theory, *J. Geophys. Res.*, 97, 13,853–13,864, 1992.
- Kessel, R. L., S.-H. Chen, J. L. Green, S. F. Fung, S. A. Boardsen, L. C. Tan, T. E. Eastman, J. D. Craven, and L. A. Frank, Evidence of high-latitude reconnecting during northward IMF: Hawkeye observations, *Geophys. Res. Lett.*, 23, 583–586, 1996.
- Kivelson, M. G., and C. T. Russell, *Introduction to Space Physics*, pp. 236–284, Cambridge Univ. Press, New York, 1995.
- Laakso, H., et al., Oscillations of magnetospheric boundaries driven by IMF rotations, *Geophys. Res. Lett.*, 25, 3007–3010, 1998.
- Larson, D. E., et al., Tracing the topology of the October 18–20, 1995, magnetic cloud with ~ 0.1 – 10^2 keV electrons, *Geophys. Res. Lett.*, 24, 1911–1914, 1997.
- Lee, M. A., Coupled hydromagnetic wave excitation and ion acceleration upstream of the Earth's bow shock, *J. Geophys. Res.*, 87, 5063–5080, 1982.
- Lepping, R. P., and K. W. Behannon, Magnetic field directional discontinuities, 1, Minimum variance errors, *J. Geophys. Res.*, 85, 4695–4703, 1980.
- Lepping, R. P., J. A. Jones, and L. F. Burlaga, Magnetic field structure of interplanetary magnetic clouds at 1 AU, *J. Geophys. Res.*, 95, 11,957–11,965, 1990.
- Lepping, R. P., et al., The Wind magnetic field investigation, *Space Sci. Rev.*, 71, 207–229, 1995.
- Lepping, R. P., et al., The Wind magnetic cloud and events of October 18–20, 1995: Interplanetary properties and as triggers for geomagnetic activity, *J. Geophys. Res.*, 102, 14,049–14,063, 1997.
- Lin, R. P., et al., A three-dimensional plasma and energetic particle investigation for the Wind spacecraft, *Space Sci. Rev.*, 71, 125–153, 1995.
- Low, B. C., and J. R. Hundhausen, Magnetostatic structures of the solar corona, II, The magnetic topology of quiescent prominences, *Astrophys. J.*, 443, 818–836, 1995.
- Lutsenko, V. N., and K. Kudela, Almost monoenergetic ions near the Earth's magnetosphere boundaries, *Geophys. Res. Lett.*, 26, 413–416, 1999.
- Mandt, M. E., and J. R. Kan, Electrostatic potential jump across fast-mode collisionless shocks, *J. Geophys. Res.*, 96, 21,391–21,395, 1991.
- Marubashi, K., Interplanetary magnetic flux ropes and solar filaments, in *Coronal Mass Ejections*, *Geophys. Monogr. Ser.*, vol. 99, edited by N. Crooker, J. Joselyn, and J. Feynman, pp. 147–156, AGU, Washington, D. C., 1997.
- McLean, D. J., K. V. Sheridan, R. T. Stewart, and J. P. Wild, Regular pulses from the Sun and a possible clue to the origin of solar cosmic rays, *Nature*, 234, 140–142, 1971.
- Möbius, E., D. Hovestadt, B. Klecker, M. Scholer, F. M. Ipavich, C. W. Carlson, and R. P. Lin, A burst of energetic O^+ ions during an upstream particle event, *Geophys. Res. Lett.*, 13, 1372–1375, 1986.
- Moore, T. E., W. K. Peterson, C. T. Russell, M. O. Chandler, M. R. Collier, H. L. Collin, P. D. Craven, R. Fitzenreiter, B. L. Giles, and C. J. Pollock, Ionospheric mass ejection in response to a CME, *Geophys. Res. Lett.*, 26, 2339–2342, 1999.
- Ogilvie, K. W., et al., SWE, A comprehensive plasma instrument for the Wind spacecraft, *Space Sci. Rev.*, 71, 55–77, 1995.
- Osherovich, V. A., C. J. Farrugia, and L. F. Burlaga, Dynamics of aging magnetic clouds, *Adv. Space Res.*, 13(6), 57–62, 1993.
- Osherovich, V. A., J. Fainberg, and R. G. Stone, Multi-tube model for interplanetary magnetic clouds, *Geophys. Res. Lett.*, 26, 401–404, 1999.
- Petschek, H. E., Magnetic field annihilation, in *AAS-NASA Symposium on The Physics of Solar Flares*, edited by W. N. Hess, *NASA Spec. Publ.*, SP-50, 425–439, 1964.
- Priest, E. R., *Solar Magnetohydrodynamics*, D. Reidel, Norwell, Mass., p. 125, 1987.

- Roberts, B., P. M. Edwin, and A. O. Benz, On coronal oscillations, *Astrophys. J.*, 279, 857–865, 1984.
- Shay, M. A., J. F. Drake, B. N. Rogers, and R. E. Denton, The scaling of collisionless, magnetic reconnection for large systems, *Geophys. Res. Lett.*, 26, 2163–2166, 1999.
- Skoug, R. M., et al., A prolonged He⁺ enhancement within a coronal mass ejection in the solar wind, *Geophys. Res. Lett.*, 26, 161–164, 1999.
- Smith, J. M., B. Roberts, and R. Oliver, Ducted fast waves in coronal loops: Curvature effects, *Astron. Astrophys.*, 317, 752–760, 1997.
- Smith, Z., S. Watari, M. Dryer, P. K. Manoharan, and P. S. McIntosh, Identification of the solar source for the 18 October 1995 magnetic cloud, *Sol. Phys.*, 171, 177–190, 1997.
- Sonnerup, B. U. Ö., Magnetic-field re-connexion in a highly conducting incompressible fluid, *J. Plasma Phys.*, 4, 161–174, 1970.
- Sonnerup, B. U. Ö., and L. J. Cahill Jr., Magnetopause structure and attitude from Explorer 12 observations, *J. Geophys. Res.*, 72, 171–183, 1967.
- Takeuchi, T., T. Araki, R. P. Lepping, T. Yamamoto, S. Kokubun, T. Nagai, and T. Iyemori, A magnetic cloud with unusual structure and corresponding bow shock movement observed on May 13, 1995, *Geophys. Res. Lett.*, 25, 3269–3272, 1998.
- Wu, S. T., W. P. Guo, and J. F. Wang, Dynamical evolution of a coronal streamer-bubble system, 1, A self-consistent planar magnetohydrodynamic simulation, *Sol. Phys.*, 157, 325–348, 1995.
- M. R. Collier and R. Fitzenreiter, Space Sciences Directorate, NASA Goddard Space Flight Center, Code 692, Greenbelt, MD 20771. (mcollier@pop6000.gsfc.nasa.gov; rjf@leprjf.gsfc.nasa.gov)
- W. M. Farrell, Space Sciences Directorate, NASA Goddard Space Flight Center, Code 695, Greenbelt, MD 20771. (farrell@faltraz.gsfc.nasa.gov)
- G. Gloeckler and D. C. Hamilton, Department of Physics, University of Maryland, College Park, MD 20742-2425. (gloeckler@umdsp.umd.edu; hamilton@umdsp.umd.edu)
- G. C. Ho, Applied Physics Laboratory, The Johns Hopkins University, 11100 Johns Hopkins Road, Laurel, MD 20723. (george.ho@jhuapl.edu)
- D. Larson, Space Sciences Laboratory, University of California, Berkeley, Berkeley, CA 94720-7450. (davin@ssl.berkeley.edu)
- R. P. Lepping, J. A. Slavin, and A. Szabo, Space Sciences Directorate, NASA Goddard Space Flight Center, Code 696, Greenbelt, MD 20771. (rpl@leprpl.gsfc.nasa.gov; jslavin@pop600.gsfc.nasa.gov; aszabo@pop600.gsfc.nasa.gov)
- L. Ofman, Laboratory for Astronomy and Solar Physics, NASA Goddard Space Flight Center, Code 682, Greenbelt, MD 20771. (ofman@waves.gsfc.nasa.gov)
- B. Thompson, Space Sciences Directorate, NASA Goddard Space Flight Center, Code 682, Greenbelt, MD 20771. (thompson@ktaadn.gsfc.nasa.gov)

P. Bochsler, Physikalisches Institut, University of Bern, Sidlerstrasse 5, Bern CH-3012, Switzerland. (peter.bochsler@phim.unibe.ch)

(Received February 11, 2000; revised May 8, 2000; accepted June 14, 2000.)